Atherosclerosis 286 (2019) 71–78

Contents lists available at ScienceDirect

Atherosclerosis

journal homepage: www.elsevier.com/locate/atherosclerosis

Confirmation of *Ath26* locus on chromosome 17 and identification of *Cyp4f13* as an atherosclerosis modifying gene

Juying Han, Peggy Robinet, Brian Ritchey, Heather Andro, Jonathan D. Smith*

Department of Cellular & Molecular Medicine, Cleveland Clinic, Cleveland, OH, 44122, USA

HIGHLIGHTS

- The DBA/2 mouse strain interval on chromosome 17 was confirmed to increase atherosclerosis.
- *Cyp4f13* gene was selected as the top candidate gene in this interval via transcriptomics.
- *Cyp4f13* gene knockout led to smaller atherosclerosis lesions.
- Cyp4f13 protein had omega hydroxylase activity on leukotriene B4.

ARTICLE INFO

Keywords:
Atherosclerosis
Cytochrome P-450 enzyme system
Leukotriene B4
Inflammation

ABSTRACT

Background and aims: We previously demonstrated that *Apoe*$^{-/-}$ mice on DBA/2 *vs.* AKR genetic background have > 10-fold larger atherosclerotic lesions. Prior quantitative trait locus mapping via strain intercrossing identified a region on chromosome 17, *Ath26*, as the strongest atherosclerosis-modifying locus. We aimed to confirm *Ath26*, identify candidate genes, and validate the candidate gene effects on atherosclerosis.
Methods: We bred chromosome 17 interval congenic mice to confirm that *Ath26* locus contains atherosclerosis modifying gene(s). Bone marrow derived macrophage transcriptomics was performed to identify candidate genes at this locus whose expression was correlated with lesions in a strain intercross. The *Cyp4f13* candidate gene was tested via a gene knockout approach and *in vivo* and *ex vivo* phenotype analyses.
Results: A congenic mouse strain containing the DBA/2 interval on chromosome 17 on the AKR *Apoe*$^{-/-}$ background demonstrated that this interval conferred increased lesion area. Transcriptomic analysis of bone marrow macrophages identified that expression of the *Cyp4f13* gene, mapping to this locus, was highly associated with lesion area in an F2 cohort. AKR *vs.* DBA/2 macrophages had less *Cyp4f13* mRNA expression, and their livers had lower leukotriene B4 (LTB4) 20-hydroxylase enzymatic activity. A *Cyp4f13* knockout allele was bred onto the DBA/2 *Apoe*$^{-/-}$ background and this conferred less enzymatic activity, decreased macrophage migration in response to LTB4, and smaller aortic root atherosclerotic lesions.
Conclusions: Allelic differences in the *Cyp4f13* gene may in part be responsible for the *Ath26* QTL conferring larger lesions in DBA/2 *vs.* AKR *Apoe*$^{-/-}$ mice.

1. Introduction

Mice are resistant to atherosclerosis due to low levels of apoB-containing VLDL and LDL lipoproteins and high levels of HDL. Through gene engineering and other approaches, hyperlipidemic mice have been created that are susceptible to atherosclerosis. Apolipoprotein E-deficient (*Apoe*$^{-/-}$) mice created in 1992 were the first gene knockout mouse to display hyperlipidemia and atherosclerotic lesions in the aortic root, arc, and descending aorta, even if fed a chow diet [1]. It was recognized early on that classical mouse genetics might be able to identify atherosclerosis modifier genes; and, apoE deficiency was back crossed onto several inbred strains that demonstrated large strain effects on lesion area [2]. DBA/2 *Apoe*$^{-/-}$ mice have > 10-fold larger lesions than AKR mice, in 16 week old mice fed a chow diet. Thus, we previously performed two independent strain intercrosses between these strains, assessing aortic root lesion areas in chow fed 16-week old

Abbreviations: *Apoe*$^{-/-}$, apolipoprotein E-deficient; QTL, quantitative trait locus; LTB4, leukotriene B4; ES, embryonic stem; WT, wild type; Het, heterozygous knockout; KO, homozygous knockout; BMDM, bone marrow derived macrophage; Polr2a, RNA polymerase II subunit

* Corresponding author. , Cleveland Clinic Box NC-10, 9500 Euclid Avenue, Cleveland, OH, 44195, USA
E-mail address: smithj4@ccf.org (J.D. Smith).

https://doi.org/10.1016/j.atherosclerosis.2019.05.007
Received 30 October 2018; Received in revised form 28 March 2019; Accepted 8 May 2019
Available online 09 May 2019
0021-9150/ © 2019 Elsevier B.V. All rights reserved.

mice, and used quantitative trait locus (QTL) mapping to identify atherosclerosis modifier loci on chromosomes (chr) 2, 15, and 17, which were named *Ath22*, *Ath28*, and *Ath26*, respectively [3]. The *Ath26* chr 17 locus had the strongest association with lesion area, and the goal of the present work was to confirm this locus effect on atherosclerosis through the generation of a congenic strain, identify a candidate gene within this interval, and validate its effect on atherosclerosis *in vivo*.

2. Materials and methods

2.1. Statement of animal care regulation standards

All mouse studies were performed as approved by the Cleveland Clinic Institutional Animal Care and Use Committee.

2.2. Generation of AKR.DBA/2^{chr17} congenic mice

AKR/J and DBA/2J mice on *Apoe*$^{-/-}$ background were previously described [3]. These mice were intercrossed to generate F1 mice, which were backcrossed to AKR/J *Apoe*$^{-/-}$ for 7 generations with selection for DBA/2 alleles at two AKR-DBA/2 polymorphic SNP markers (rs13459151 and rs49841774) flanking the atherosclerosis QTL on chr 17. These SNP markers were genotyped using Applied Biosystems TaqMan Universal PCR Master Mix and SNP specific primer probe sets to select mice heterozygous for the chr 17 interval. To determine the actual congenic break point and to confirm no contamination on other chromosomes, mouse SNP microarray genotyping was performed by the University of North Carolina Systems Genetics core using the MegaMUGA platform. The chr 17 heterozygous mice were brother and sisters mated to generate three genotypes of male and female AA, AD and DD in the congenic interval for the atherosclerosis assay of aortic root lesion quantification.

2.3. Determination of eQTL with F2 mice on Ch17 Ath26

Bone marrow derived macrophage (BMDM) transcriptomic analysis was performed in F2 mice derived from an AKR/J x DBA/2J *Apoe*$^{-/-}$ strain intercross using Affymetrix mouse expression arrays as previously described [3]. From this published BMDM gene expression data (GEO accession # GSE35676), we correlated lesion areas in the F2 mice with each BMDM expressed transcript.

2.4. Generation of Cyp4f13 knock-out mouse

To test the effects of *Cyp4f13* gene on atherosclerosis, we obtained *Cyp4f13* knock-out (KO) mice. *Cyp4f13* KO embryonic stem (ES) cells were made by Lexicon (clone OST14770). Details are described in Supplemental Materials. *Cyp4f13* hemizygous mice on the DBA/2 *Apoe*$^{-/-}$ background were brother sister mated to generate male and female mice of the three genotypes: wild type (WT), heterozygous (Het) and homozygous (KO) at the expected 1:2:1 ratio. Additional WT and KO mice were generated by breeding within these genotypes.

2.5. Determination of gene expression of Cyp4f13 by real-time PCR

BMDM were cultured for ~14 days in BMDM culture media (DMEM containing 15% FBS and 20% L-cell conditioned media as a source of M-CSF) until the cells were fully differentiated at 85–95% confluency. BMDM were isolated from four types of mice: *Cyp4f13* WT, Het, and KO on the DBA/2, as well as AKR/J mice on *Apoe*$^{-/-}$ background. Total RNA was extracted from these cells using miRNA mini kit from QIAGEN. 1 μg of RNA from each sample was used to make cDNA using the iScript Advanced cDNA Synthesis Kit from Bio-Rad. Real-time PCR assay was performed with Applied Biosystems TaqMan Universal PCR Master Mix and Taqman probe Mouse Chr 17: Mm00504576_M1 (Chr17:32924688–32947415 on Build GRCm38) (Thermo Fisher Scientific). 1 μl of cDNA was applied to the real-time PCR assay. A standard reaction protocol was followed: 50 °C for 2 min, 95 °C for 10 min, 40 cycles of 95 °C for 15 s and 60 °C for 1 min. Relative gene expression in each sample compared to WT mouse BMDM was performed by the ΔΔCт method using mouse Polr2a (RNA polymerase II subunit) as endogenous control. The results were expressed as $2^{-\Delta\Delta C_T}$ for the fold changes in expression.

2.6. Atherosclerosis assay: quantification of aortic root lesion area and lesion composition

Male and female mice of three genotypes of chr 17 interval congenic mice AA, AD and DD on the AKR/J background, and male and female mice of the three genotypes for *cyp4f13* WT, Het and KO on DBA/2J *Apoe*$^{-/-}$ background were fed a chow diet (Teklad 2018). Mice were sacrificed by CO_2 inhalation and weighed at 16 weeks of age. Whole blood was collected from the retroorbital plexus into a heparinized glass capillary and transferred to a tube containing 2 μl EDTA, which was spun in a microfuge to obtain plasma. The circulatory system was perfused with 10 mL PBS and the heart was excised and preserved in 10% phosphate buffered formalin (Thermo Fisher Scientific). Quantitative assessment of atherosclerosis in the aortic root was performed as previously described [4]. Lesion areas were quantified as the mean value in six sections at 80 μm intervals using Image Pro software (Media Cybernetics). In order to assess lesion composition, and additional cohort of 3 male *cyp4f13* WT and KO on DBA/2J *Apoe*$^{-/-}$ background were fed a chow diet and sacrificed at 16 weeks of age. The unfixed hearts from these mice were fresh frozen in OCT and 10 μm sections were cut through the aortic root. Sections were fixed with acetone for 10 min at room temperature. For macrophage staining, sections were blocked with 5% BSA in PBS for 1 h at 37 °C, and the primary antibody anti-mouse CD68 (MAC1957GA, Bio-Rad, 1:50 diluted in 1% BSA in PBS) was incubated at 37 °C for 1 h. The secondary antibody, TRITC-conjugated AffiniPure Mouse anti-rat IgG (121-025-082, Jackson Immunoresearch Laboratories, 1:100 dilution in 1% BSA in PBS) was Incubate at 37 °C for 30 min. For smooth muscle staining, serial sections were blocked with Casein Blocker (37532, Thermo Scientific) for 1 h at 37 °C, and the anti-actin mouse monoclonal conjugated with Cy3 (C6198, Sigma-Aldrich, diluted 1:100 in Caseins blocker) was incubated for 1 h at 37 °C. Slides were Vectashield containing DAPI (H-1200, Novus Biologicals) for nuclear staining. For lesion necrosis, serial sections were stained with hematoxylin for 15 min at room temperature. For each mice up to 3 lesions were quantified for macrophage area, smooth muscle cell area, and necrotic area, represented as the % lesion area for each lesion.

2.7. Determination of total cholesterol and HDL-cholesterol

30 μl of plasma was mixed with 30 μl of KBr (density of 1.12 g/mL), placed into 0.2 mL tubes and centrifuged at 70,000 rpm for 16 h in an S100-AT3 rotor (Thermo Fisher Scientific). The bottom 30 μl layer with a density > 1.063 was used to determine HDL-cholesterol, and the plasma 10X diluted with PBS was used for testing total cholesterol levels, both run with technical duplicates using the Cholesterol Liquicolor kit (StanBio Laboratory, #1010–225) adapted to a 96 well plate format.

2.8. Characterization of peritonitis induced by zymosan injection

Two groups of age matched WT and KO on DBA/2J *Apoe*$^{-/-}$ background female mice were injected i.p. with a zymosan suspension based on mouse body weight (70 μg zymosan/g body weight). 0, 4, or 6 h after zymosan injection the mice were euthanized by CO_2. Peritoneal lavage was performed using 4 mL PBS. The lavage fluid volume was measured and centrifuged for 5 min at 700 rpm at 4 °C. The supernatant was saved for measuring LTB4 levels by ELISA (R&

DSystems, #KGE006B). The cell pellets were suspend in 200 µl PBS. 2 mL of 1XRBC Lysis Buffer (Invitrogen) was added to the cell suspension kept on ice for 5 min, then 5 mL of PBS was added. Samples were centrifuged at 700 rpm at 4 °C for 5 min and the cell pellets were re-suspended in 1 mL of PBS for cell counting in a Coulter Counter.

2.9. Determination of LTB4 hydrolase activity in mouse liver by LC-MS/MS

Mouse liver microsomes were prepared and assayed by mass spectrometry for LTB4 20 hydroxylation using a deuterated LTB4 substrate and internal standards, as described in Supplemental Materials.

2.10. Bone marrow derived mouse macrophage migration assay

BMDM from DBA/2J WT and KO mice on *Apoe*$^{-/-}$ background were plated into 24 well plates. A scratch line was made with a 1 mL pipette tip when the cells were fully differentiated and 85–95% confluent at day 10–14. The wells were washed 3x with PBS to remove floating cells. Three conditions were used to treat the cells, serum-free DMEM plus M-CSF (10 ng/mL) as a negative control, serum-free DMEM plus M-CSF plus LTB4 (300 nM), and serum-containing BMDM culture medium as a positive control, with each condition used in triplicate wells. Since we did not include an inhibitor of cell proliferation in this assay, a portion of the cell migration into the scratch may be due to cellular proliferation. Lines were drawn on the bottom of the wells to uniquely define each scratch segment and as fiduciary landmarks that were used later to align the images at two time points. Two to four segments of each scratch in each well were analyzed. Images were taken at time 0 h immediately after adding the treatment condition to each well. The plates were incubated at 37 °C for 24 h and images of same area of each segment were obtained. The images (0 and 24 h) were edited with PhotoShop and false colors were applied to distinguish the 0 and 24 h time points. The two images of each segment were aligned via the fiduciary landmarks and superimposed using a blending option to adjust the layer opacity until the two layers were clearly identified showing the scratch boundary at 0 and 24 h time points. The distance of cell migration was determined 8–10 times within each segment on both sides of the scratch. Data from segments where migration from the two sides of the scratch were not similar (> 24% deviation) were eliminated.

2.11. Bone marrow derived macrophage AcLDL uptake, cholesterol loading, and cholesterol efflux

Human LDL (1.019 < d < 1.063 g/mL) and human HDL (1.063 < d < 1.21 g/mL) were prepared by ultracentrifugation. LDL was acetylated as described previously [5,6]. HDL, LDL and AcLDL were dialyzed against PBS with 100 µM EDTA and 20 µM BHT. For DiI (1,1′-dioctadecyl-3,3,3′,3′-tetramethylindocarbocyanine perchlorate) labeling, 10 mg/mL DiI stock in DMSO was diluted in PBS and added to AcLDL at a final concentration of 10 µg/mg of protein. The mixture was incubated at 37 °C for 25min and centrifuged for 2min to pellet any insoluble debris. The supernatant was collected and filtered sterilized before use. For [3H] labeling, [3H]-cholesterol in ethanol was pre-incubated with undiluted AcLDL at a final concentration of 0.5 µCi/mL for 30 min at 37 °C before adding to DMEM at a final concentration of 50 µg/mL AcLDL. To measure DiI-AcLDL uptake, WT and KO BMDM in 24-wells plates were incubated in DMEM containing 50 µg/mL DiI-labeled AcLDL for 1 h at 37 °C. The cells were detached from the plate using Cell Stripper (Cellgro). The cells were resuspended and analyzed by flow cytometry (LSRII, Becton-Dickinson). Fluorescence was gated for individual live cells and the fluorescence associated with 10,000 cells was determined for each sample. The data collected from the cells were analyzed with Flowjo software. To measure cholesterol loading, WT and KO BMDM in 12-well plates were incubated for 16 h at 37 °C with culture media with or without 50 µg/mL AcLDL. The cells were washed and cholesterol was extracted from cells using hexane:isopropanol (3:2; v:v) and protein extracted using 0.2N NaOH/0.2% SDS. Total, free and esterified cholesterol as well as protein mass were evaluated as described previously [7]. To measure cholesterol efflux, WT and KO BMDM were cholesterol labeled with 50 µg/mL [3H]-AcLDL in DMEM containing 10 ng/mL MCSF for 16 h at 37 °C. After labeling, cells were chased for 4 h at 37 °C in DMEM with or without acceptors (5 µg/mL apolipoprotein AI or 100 µg/mL HDL). At the end of this chase period, the radioactivity in the medium and cells was determined by liquid scintillation counting, and the percent efflux was calculated as [100 x (medium dpm)]/(medium dpm + cell dpm). Percent efflux to acceptors was calculated as (percent efflux in presence of acceptors)-(percent efflux in absence of acceptors).

2.12. Statistics

All statistics were performed using GraphPad Prism software. Tests for normal data distribution were performed before analyzing for group differences and non-normally distributed data were analyzed using nonparametric statistical tests. Comparisons of two groups were made by *t*-test and of more than two groups by ANOVA with the specified posttest. Values shown are mean ± SD unless indicated otherwise. For *Cyp4f13* knockout mouse studies, a pre-specified outlier removal process was applied: if a data point was > 2 SD away from the remaining data, that data was removed as an outlier and specified in the figure legend.

3. Results

3.1. Confirmation of the Ath26 locus on chr 17 and identification of the candidate gene Cyp4f13

Our two prior AKR/JxDBA/2J *Apoe*$^{-/-}$ strain intercrosses yielded F2 mice from which we measured atherosclerosis lesion areas and strain specific markers throughout the genome, allowing us to identify three genome-wide significant AthQTL loci on chr 2, 15, and 17, with the chr 17 locus, named *Ath26* [3,8]. The confidence interval for this locus was very large, spanning from 12.3 to 64.3 Mb on chr 17 [3]. At that time, we also measured BMDM gene expression using expression microarrays, and identified that many of the BMDM expressed genes were associated with strain specific *cis*-genetic variation, which are called *cis*-expression quantitative trait loci, or *cis*-eQTLs. In the *Ath26* QTL interval, we identified several genes with significant *cis*-eQTLs, among them was the *Cyp4f13* gene, at 32.7 Mb on chr 17 with strong *cis*-eQTLs in both male and female F2 mice (LOD 11.6 and 7.4, respectively) [9]. We revisited the gene expression and atherosclerosis data from that prior F2 cross and performed a correlation analysis for gene expression *vs.* atherosclerosis lesion area. In the male mice, the strongest gene expression-lesion correlation was found for the *Cyp4f13 gene* (Fig. 1A, r = 0.46, $r^2 = 0.21$, $p < 0.0001$). *Cyp4f13* expression in male F2 mice divided into three genotypes at the *Cyp4f13* locus is shown in Fig. 1B; and there was a significant additive genotype effect on *Cyp4f13* expression levels, with the DBA/2 genotype associated with higher expression, such that the AKR allele was expressed on average 43% lower than the DBA/2 allele. We confirmed via qPCR that AKR BMDM expressed less *Cyp4f13* mRNA than DBA/2 BMDM (Figs. 1C and 38% lower in AKR, $p < 0.01$ by ANOVA posttest). Additionally, we found a nonsynonymous variant at residue 453 in the Cyp4f13 protein, with a Ser residue in the DBA/2 strain and a Pro residue in the AKR strain; and this change is predicted to alter protein function as determined by Polyphen2 analysis [3].

In order to confirm the *Ath26* QTL, we backcrossed F1 mice onto the AKR *Apoe*$^{-/-}$ strain to create congenic mice maintaining the DBA chr 17 segment from 32.82 to 66.71 Mb on the AKR genetic background (mouse NCBI37/mm9 genome build). Atherosclerosis lesion areas in female congenic mice revealed that mice inheriting two DBA/2 alleles (DD) at this locus had significantly larger lesions than those with 1 (DA)

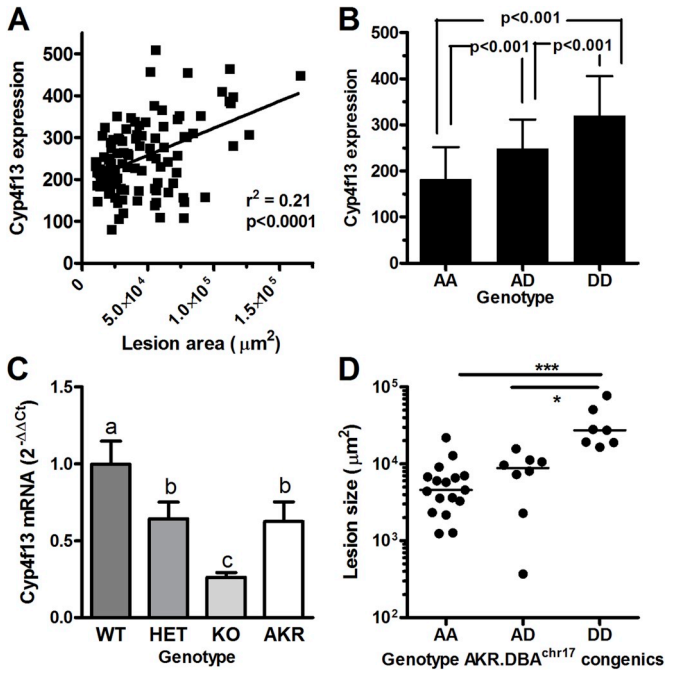

Fig. 1. Confirmation of the *Ath26* locus on chr 17 and identification of the candidate gene *Cyp4f13*.
(A) Correlation between lesion area and *Cyp4f13* gene expression in BMDM from F2 male mice (n = 114, r = 0.46, r^2 = 0.21, $p < 0.0001$). (B) F2 male mice were divided into three genotypes AA (n = 24), AD (n = 62), DD (n = 27) at the *Cyp4f13* locus. BMDM from three genotypes were cultured and *Cyp4f13*expression was determined by microarray (p values < 0.001 by ANOVA analysis with Tukey posttest). (C) *Cyp4f13* gene expression assessed by qPCR in BMDM from the DBA/2J WT, Het and KO as well as AKR/J mice (n = 3 to 4 biological replicates, different letters above the bars represent $p < 0.05$ by ANOVA with Tukey posttest). (D) Aortic root lesion areas confirm the *Ath26* QTL in female congenic mice on the AKR background. The genotype of the chr 17 interval is designated as homozygous for DBA/2 (DD, n = 8), heterozygous (AD, n = 10), and homozygous for AKR (AA, n = 17) (*, $p < 0.05$; ***, $p < 0.001$ by nonparametric ANOVA with Dunns posttest).

or 0 (AA) DBA/2 allele (Fig. 1D). The median lesion area in the DD genotype congenic females was > 5-fold larger than in the AA genotype congenic females. There was no effect of the congenic interval genotype on total or HDL cholesterol levels in female mice (not shown). We also assessed lesion areas in male congenic mice, and due to smaller number of mice and larger variance, the differences were not significant; however, the same trend was apparent with the median lesion are 3.5-fold larger in the DD *vs.* AA genotype congenic males (not shown).

3.2. Characterization of Cyp4f13 KO mice

We obtained mouse ES cells with a deletion of the final coding exon of the *Cyp4f13* gene, as described in the Methods section, and we refer to this as the KO allele, although a truncated protein may be expressed. Mice were generated from these ES cells and bred onto the DBA/2 *Apoe*$^{-/-}$ background. As shown in Fig. 1C, we prepared RNA from BMDM of DBA/2 WT, Het, and KO mice and found that *Cyp4f1*3 mRNA expression in KO mice was significantly decreased compared with WT (71% decreased). *Cyp4f13* expression in Het BMDM was significantly different and intermediate between WT and KO levels, and equal to the expression level in the AKR BMDM.

We measured an enzymatic activity of Cyp4f13, the omega hydroxylation of leukotriene B4 (LTB4) to 20-OH-LTB4, using liver microsomes from male DBA/2 WT, Het, KO, and AKR/J mice *Apoe*$^{-/-}$ background. Microsomal cytochrome P450 (Cyp450) dependent enzymatic reactions were performed with the addition of the deuterated

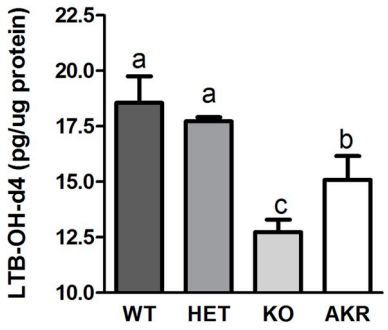

Fig. 2. LTB4 20-hydroxylase activity.
Omega hydroxylation of LTB4 to 20-OH-LTB4 was measured in a 30 min incubation with liver microsomes from male DBA/2 WT, Het, KO, and AKR/J mice (n = 3 per genotype, different letters above the bars represent columns with $p < 0.05$ by parametric ANOVA with Newman–Keuls posttest).

leukotriene B4 (d4-LTB4) substrate. Compared to the DBA/2 WT microsomes, the HET and KO microsomes had 8% and 25% less activity, respectively (Fig. 2). AKR *vs.* DBA/2 microsomes also had 8% less activity. We suspect that the reason that the activity was impaired less than the mRNA levels is that there are other related *cyp4f* genes that also have LTB4 omega hydroxylase activity.

3.3. Bone marrow derived macrophage migration

To determine if the *Cyp4f13* KO altered a biological response in BMDM, we performed a scratch wound 24-h cell migration assay using LTB4 or serum as migration agonists. The WT and KO BMDM derived from female mice migrated to the same extent in serum-free control media containing 10 ng/ml M-CSF, needed to maintain cell viability. Serum-containing BMDM growth media induced increased migration in both the WT and KO BMDM, with no difference in the migration distance between cell types. However, the addition of 300 nM LTB4 led to a 12% significant increase in migration in WT cells, but a non-significant 5.5% increase in KO cells (Fig. 3A). Thus, KO cells with less LTB4 20-hydroxylase activity are less responsive to LTB4 agonist.

3.4. Bone marrow macrophage cholesterol metabolism

We measured DiI-labeled AcLDL uptake by WT and KO BMDM by flow cytometry, and found no difference in the median fluorescence intensity (MFI, 4830 ± 405, 5095 ± 239 mean ± SD for WT and KO, respectively, n = 5). After [^{3}H]cholesterol loading and labeling BMDM, we measured cholesterol efflux to apoA1 and HDL acceptors. There was no genotype effect on efflux to apoA1; however, there was a 21% significant increase in efflux to HDL from the KO *vs.* WT BMDM (Fig. 3B). We then measured total, free, and esterified cholesterol (TC, FC, and CE, respectively) in unloaded and AcLDL loaded BMDM. AcLDL loading significantly increased TC, FC, and CE in both genotypes. However, the KO *vs.* WT BMDM had decreased TC and CE mass after AcLDL loading, with no effect on FC (Fig. 3C–E).

3.5. Zymosan induced peritonitis

We subjected WT and KO female mice to zymosan i.p. injection and performed peritoneal lavage at 0 (untreated) 4, and 6 h afterwards. Total cell number in the lavage fluid was markedly induced at 4 h and still rising at 6 h (Fig. 4A). Two-way ANOVA analysis showed a significant effect of time, but no effect of genotype or interaction between time and genotype. We also measured LTB4 levels in the peritoneal lavage supernatant, and it peaked at 4 h, but was still elevated at 6 h (Fig. 4B). Two-way ANOVA analysis showed a significant effect of time, and a non-significant trend for genotype ($p = 0.07$), with 58% more LTB4 measured at 4 h in the KO mice, such that there was a significant

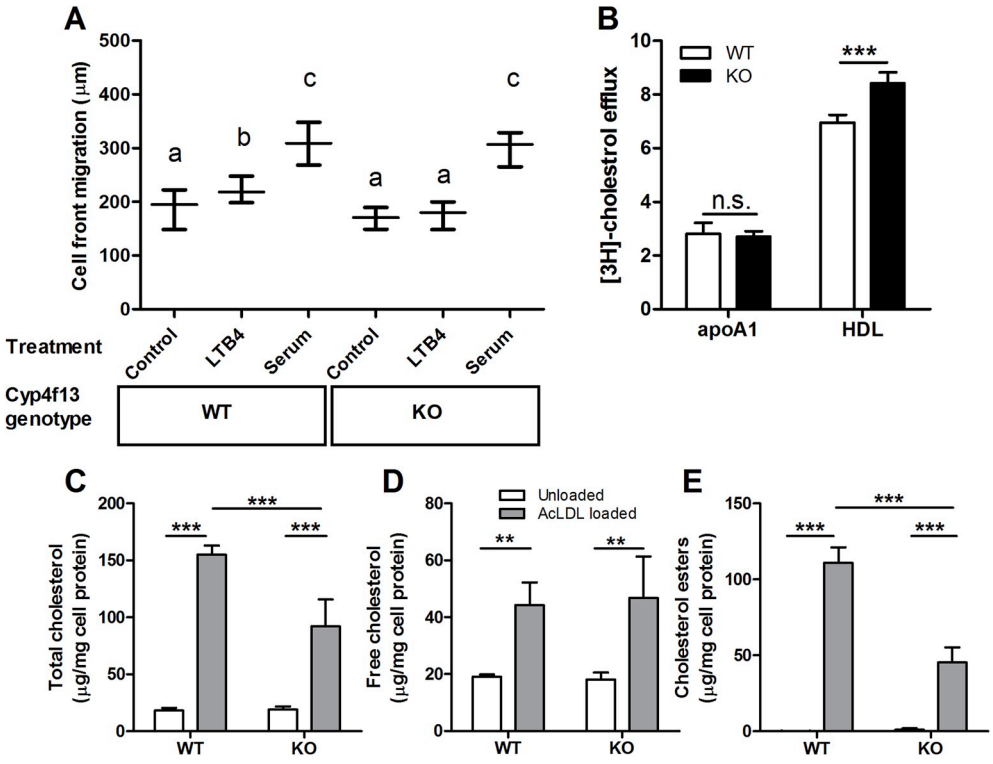

Fig. 3. Macrophage migration and cholesterol metabolism.
(A) WT and *Cyp4f13* KO BMDM 24 h migration after scratch wound in response to LTB4 (300 nM) or 15% serum-containing media. Migration distance was measured at multiple positions along multiple scratches for each condition (medium ± interquartile range, > 100 measurements made for each condition, different letters above the data represent columns with $p < 0.05$ by nonparametric ANOVA with Dunns posttest). (B) Cholesterol efflux from WT and *Cyp4f13* KO BMDM to apoA1 and HDL acceptors (n = 4 for each condition). (C–E) Total, free, and esterified cholesterol levels in unloaded (open bars) and AcLDL loaded (gray bars) WT and *Cyp4f13* KO BMDM, normalized to cell protein (n = 4 per condition). For (B–D), **, $p < 0.01$; ***, $p < 0.001$ by parametric ANOVA with Newman–Keuls posttest.

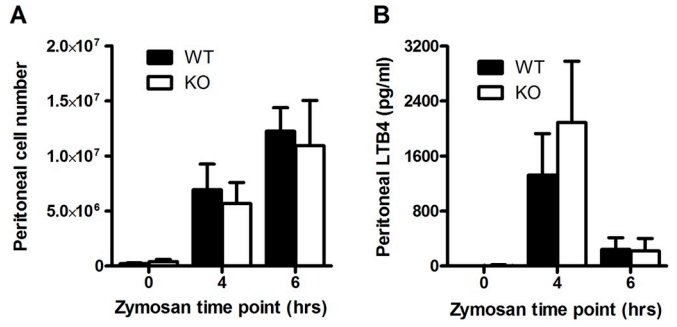

Fig. 4. Zymosan induced peritonitis.
Peritoneal cell number (A) and LTB4 levels (B) were measured at 0, 4, and 6 h after female mice were injected i.p. with zymosan. Two-way ANOVA analysis for cell number found a time effect ($p < 0.0001$), but no genotype or interaction effects (n = 3 to 6 per genotype at each time point). Two-way ANOVA analysis for LTB4 levels found a time effect ($p < 0.0001$), a trend for a genotype effect ($p = 0.07$), and an interaction effect ($p = 0.035$, n = 4 to 10 per genotype at each time point).

interaction between time and genotype ($p = 0.035$). The increase in LTB4 levels at 4 h is consistent with less 20-hydroxylase activity in the KO mice, although this had no significant effect on recruitment of leukocytes into the peritoneal cavity.

3.6. Atherosclerosis

To determine the effect of *Cyp4f13* genotype on the formation of aortic root atherosclerosis, male and female WT, Het, and KO mice on DBA/2 *Apoe*$^{-/-}$ background were fed with chow diet and sacrificed at 16 weeks of age. Since sex can affect lesion area in mouse models [10], we analyzed atherosclerosis separately in the two sexes. In the female mice, the *Cyp4f13* Het mice (n = 18) and KO (n = 13) mice had significantly smaller lesions than the WT mice (n = 17) ($p < 0.001$ and $p < 0.05$, respectively by ANOVA with Tukey's posttest). There was no significant difference in lesion area between the HET and KO mice, and lesions were on average 35% smaller in the KO *vs.* WT female mice (Fig. 5A). A similar effect was observed in the male mice where HET (n = 16) and KO (n = 25) lesion areas were significantly smaller than in WT (n = 11) mice ($p < 0.05$ for both comparisons by ANOVA with Tukey's posttest). In a separate study, we evaluated lesion composition in serial sections of the aortic root by evaluating macrophage and smooth muscle cell content by immunostaining against CD68 and alpha actin, respectively, and necrotic area by hematoxylin staining (Fig. 5C). These early lesions on chow diet fed mice consist primarily of macrophages; although there was some smooth muscle cell and necrotic areas as well. Cyp4f13 genotype had no effect on macrophage or smooth muscle cell relative area, but necrotic relative area was significantly increased in the KO mice, despite the overall smaller lesion area in these mice. There was no significant genotype differences on plasma total cholesterol, HDL-cholesterol, or nonHDL-cholesterol levels or the ratio of non-HDL/HDL-cholesterol in the female or male mice (Table 1). Thus, reduced Cyp4f13 activity was associated with decreased atherosclerosis, independent of an effect on plasma cholesterol levels, indicating that the strain effect of expression of this gene may contribute to the *Ath26* QTL locus on chr.17.

4. Discussion

Our unbiased genetic approach via a mouse strain intercross identified an atherosclerosis modifier locus on chr 17, which we confirmed by generation of a congenic strain. Our transcriptomic analysis of F2 macrophages found that expression of the *Cyp4f13* gene, which resides in the chr 17 interval, had the strongest correlation with lesion area in the F2 mice, making this the top candidate gene. The mouse *Cyp4f* gene family consists of 9 related genes, 8 clustered on chr 17 and one on chr 8. This gene family is known to have ω-hydroxylation activity for polyunsaturated fatty acids as well as for eicosanoids and LTB4 [11]. The gene names are not consistent in mice and humans, and the closest homologue of mouse *Cyp4f13* is human *CYP4F11*. Although there are no detailed substrate studies for the mouse Cyp4f13 protein, the human CYP4F11 protein has been expressed in yeast and found to have efficient ω-hydroxylation activity on the saturated 16:0, the

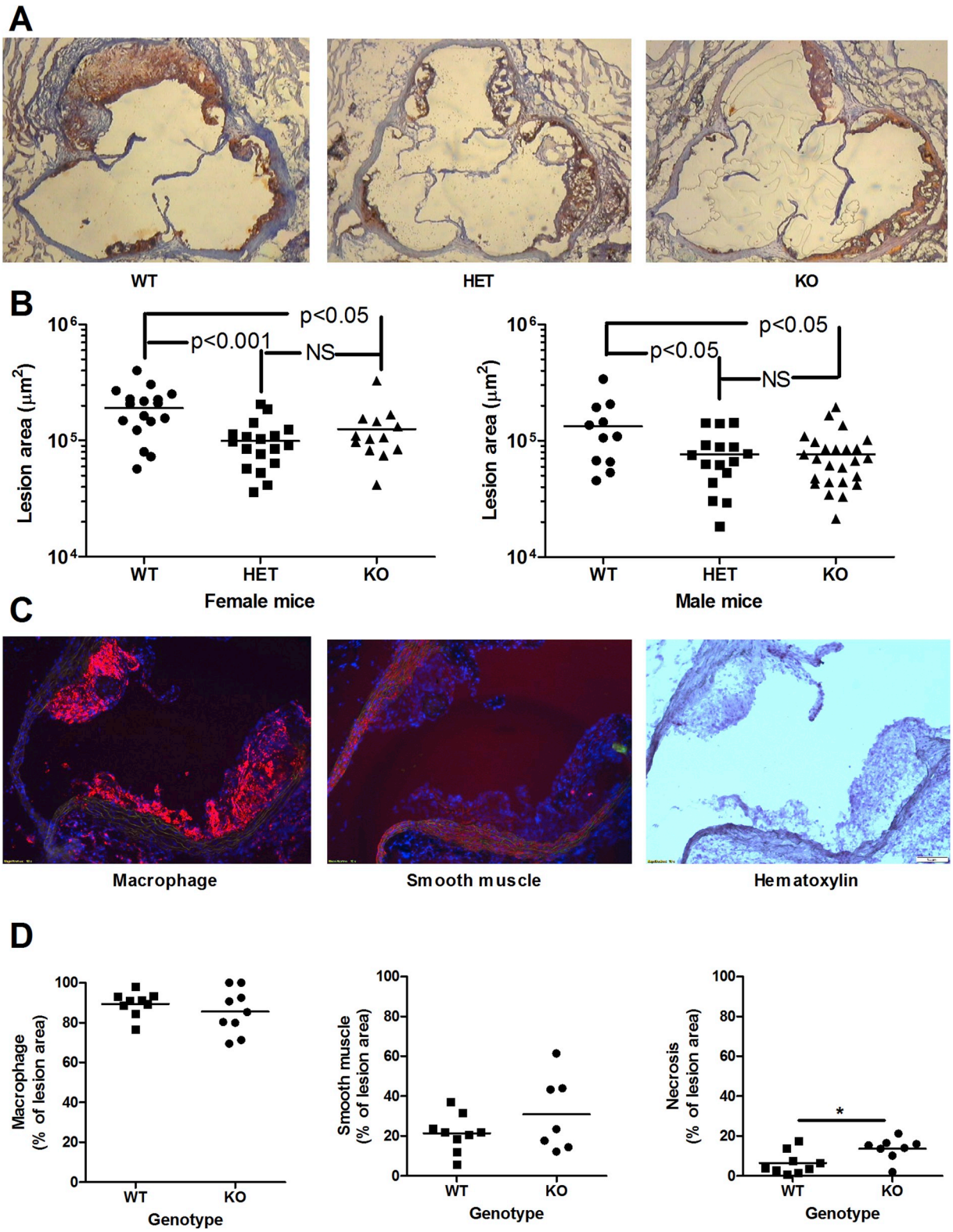

Fig. 5. C*yp4f13* genotype effect on atherosclerosis.
(A) Representative aortic root lesions stained with Oil red O and hematoxylin in 16 week old chow-diet fed female DBA/2 *Apoe*$^{-/-}$ mice of the indicated *Cyp4f13* genotype. (B). Aortic root lesion areas in female (left panel) and male (right panel) mice for the indicated *Cyp4f13* genotypes. Parametric ANOVA *p*-values are shown above the data using Tukey's posttest analysis. For the male mice, one WT and one Het values were excluded based on the pre-specified > 2 S.D. outlier rule. (C) Representative aortic root lesions stained for macrophages (left panel, CD68 immunofluorescence in red), smooth muscle cells (center panel, alpha actin immunofluorescence in red), and with hematoxylin (right panel) in order to determine lesion cellular composition and necrosis. Blue shows nuclei stained with DAPI, and green shows autofluorescence of the elastic lamina. (D) Quantification of macrophage (left panel), smooth muscle cell (middle panel), and necrotic (right panel) relative lesion areas (n = 7 to 9 lesions per genotype, $^{*}p < 0.05$).

Table 1
Plasma cholesterol values in *Apoe*$^{-/-}$ mice by sex and *Cyp4f13* genotypes.

Gender/genotype	Total cholesterol[a]	HDL-cholesterol[a]	NonHDL-cholesterol[a]	NonHDL/HDL	# of mice
Female/WT	805.8 ± 263.4	25.79 ± 11.96	780 ± 264.9	38.37 ± 26.44	18
Female/Het	847.3 ± 222.9	25.7 ± 11.54	821.6 ± 221	39.07 ± 25.78	17
Female/KO	700.2 ± 277.7	28.44 ± 14.69	671.7 ± 272	26.7 ± 14.4	10
1way ANOVA	NS	NS	NS	NS	
Male/WT	769.5 ± 213.1	45.24 ± 16.29	724.2 ± 211.1	17.98 ± 8.06	7
Male/Het	870.1 ± 185	33.58 ± 15.51	836.5 ± 184.8	29.65 ± 13.66	16
Male/KO	810.5 ± 327.5	34.73 ± 14.67	775.8 ± 320.2	24.45 ± 11.88	17
1way ANOVA	NS	NS	NS	NS	

[a] Values in mg/dl.

monosaturated 18:1, and the polyunsaturated 20:4 and 22:6 fatty acids [12]. Another group determined that CYP4F11 also has LTB4 and Lipoxin A4 ω-hydroxylase activity [13]. In addition, human CYP4F3B, its mouse homologue Cyp4f18, and mouse Cyp4f14 have also been found to have LTB4 hydroxylation activity [14–16]. Thus, there is a potential role for *Cyp4F* gene members to produce or metabolize pro-inflammatory and anti-inflammatory lipids.

Leukotrienes are a family of lipid mediators and synthesized from arachidonic acid via the 5-lipoxygenase pathway [17]. During inflammation LTB4 stimulates neutrophil activation and chemotaxis leading to degranulation and the release of antimicrobial proteins such as myeloperoxidase [18]. Cyp4F proteins are thought to inactivate LTB4 by ω-hydroxylation [19]. However, previous studies showed that the 20-OH-LTB4 also had similar chemotactic activity as LTB4 and could be a pro-inflammatory mediator as well [20,21]. Our present studies found significantly decreased 20-OH-LTB4 production by *Cyp4f13* KO mouse liver microsomes, confirming that Cyp4f13 has LTB4 ω-hydroxylation activity. We also found that BMDM from *Cyp4f13* KO mice had significantly reduced cell migration in response to LTB4. This latter finding seems contradictory to expectations if ω-hydroxylation is the first step in LTB4 catabolism. Instead, our findings suggest that 20-OH-LTB4 may be a more potent pro-inflammatory agonist than LTB4, or that its ω-hydroxylation prevents LTB4 turnover by another more rapid pathway. It has been proposed that the increased hydrophobicity of 20-OH-LTB4 *vs.* LTB4, makes it a more potent chemoattractant [20].

We also examined macrophage cholesterol metabolism, and although there was no effect of the *Cyp4f13* KO on a 1 h uptake of AcLDL, upon a longer incubation with AcLDL, the KO BMDM accumulated lower levels of total and esterified cholesterol. This effect on cholesterol accumulation may have been due to increased efflux to lipoprotein acceptors, which we also observed. Thus, during the prolonged loading period, the KO macrophages may have released more cholesterol back to the medium. In addition, cholesterol esterification or lipid droplet turnover rates may also have been affected. The decreased cholesterol loading in the KO macrophages is consistent with the observed effect on aortic root lesion area, namely smaller lesions in the KO mice.

We used a zymosan peritonitis model to determine if *Cyp4f13* KO had any effect on cellular infiltration. And although we found a trend for increased LTB4 levels 4 h after zymosan injection, we did not see any difference in leukocyte recruitment. Zymosan is a potent inducer of inflammation via several pathways including toll like receptors and dectin-1, so any effect of LTB4 on cell recruitment may be masked in this assay. The lack of an effect of *Cyp4f13* KO on zymosan peritonitis suggests that there is no effect on adhesion molecules which mediate this recruitment; however, we did not directly asses this in either macrophages or endothelial cells.

Upon breeding to *Apoe*$^{-/-}$, *Cyp4f13* Het and KO genotypes led to smaller aortic root lesions in both male and female mice. This result is congruent with the mouse strain effect in which the AKR allele, *vs.* the DBA/2 allele, is associated with lower *Cyp4f13* gene expression, lower LTB4 ω-hydroxylation activity, and smaller lesions. Although this *Cyp4f13* KO confirms this candidate gene as a causal gene, there are several limitations of our study that must also be considered. First, *Cyp4f13* might not be the only gene affecting atherosclerosis in the *Ath26* QTL interval. Further fine mapping via breeding additional congenic strains studies may help to clarify this point. Second, the *Cyp4f13* KO allele was created using strain 129 embryonic stem cells. Thus, in selection for the KO allele, adjacent 129 alleles are also retained, leading to the so called "passenger gene" effect [22]. Beyond the scope of the present study, due to the more recent availability of C57BL/6 embryonic stem cells, it would be possible to confirm the effect of *Cyp4f13* KO in C57BL/6 mice without the passenger gene limitation. In conclusion, our data support that expression of *Cyp4f13* gene is pro-atherogenic in mice, and that 20-OH-LTB4 may be a potent pro-inflammatory lipid mediator.

Conflicts of interest

The authors declared they do not have anything to disclose regarding conflict of interest with respect to this manuscript.

Financial support

This work was supported by National Institutes of Health grant P01HL029582 to J.D.S. and American Heart Association grant #15sdg25310009 to Peggy Robinet.

Author contributions

Juying Han performed the cell based studies, the *Cyp4f13* knockout mouse studies, and the mouse atherosclerosis histology, lesion composition, and analyses. She analyzed most of the data, prepared most of the figures, and wrote the first draft of the manuscript. Peggy Robinet performed the backcrossing and genetic analysis of the chr 17 congenic mice and analyzed that data. She also performed the macrophage AcLDL uptake, efflux, and cholesterol loading studies. Brian Ritchey prepared the mouse liver microsomes and performed the LTB4 omega hydroxylase activity assays by LC/MS-MS, and he wrote the methods for this assay. Heather Andro assisted with the zymosan peritonitis assays. Jonathan Smith supervised the project, raised most of the funding, and worked with Juying Han on the writing and assembly of the final manuscript.

Appendix A. Supplementary data

Supplementary data to this article can be found online at https://doi.org/10.1016/j.atherosclerosis.2019.05.007.

References

[1] A.S. Plump, J.D. Smith, T. Hayek, K. Aalto-Setala, A. Walsh, J.G. Verstuyft, E.M. Rubin, J.L. Breslow, Severe hypercholesterolemia and atherosclerosis in apolipoprotein E-deficient mice created by homologous recombination in ES cells, Cell 71 (1992) 343–353.

[2] J.D. Smith, D. James, H.M. Dansky, K.M. Wittkowski, K.J. Moore, J.L. Breslow, In silico quantitative trait locus map for atherosclerosis susceptibility in apolipoprotein E-deficient mice, Arterioscler. Thromb. Vasc. Biol. 23 (2003) 117–122, https://doi.org/10.1161/01.ATV.0000047461.18902.80.
[3] J. Hsu, J.D. Smith, Genetic-genomic replication to identify candidate mouse atherosclerosis modifier genes, J. Am. Heart Assoc. 2 (2013) 1–15, https://doi.org/10.1161/JAHA.112.005421.
[4] J. Baglione, J.D. Smith, Quantitative assay for mouse atherosclerosis in the aortic root, Methods Mol. Med. 129 (2006) 83–96, https://doi.org/10.1385/1-59745-213-0:83.
[5] H. Fraenkel-Conrat, Methods for investigating the essential groups for enzyme activity, Methods Enzymol. 4 (1957) 247–269, https://doi.org/10.1016/0076-6879(57)04059-8.
[6] S.K. Basu, J.L. Goldstein, G.W. Anderson, M.S. Brown, Degradation of cationized low density lipoprotein and regulation of cholesterol metabolism in homozygous familial hypercholesterolemia fibroblasts, Proc. Natl. Acad. Sci. 73 (2006) 3178–3182, https://doi.org/10.1073/pnas.73.9.3178.
[7] P. Robinet, Z. Wang, S.L. Hazen, J.D. Smith, A simple and sensitive enzymatic method for cholesterol quantification in macrophages and foam cells, J. Lipid Res. 51 (2010) 3364–3369, https://doi.org/10.1194/jlr.d007336.
[8] J.D. Smith, J.M. Bhasin, J. Baglione, M. Settle, Y. Xu, J. Barnard, Atherosclerosis susceptibility loci identified from a strain intercross of apolipoprotein E-deficient mice via a high-density genome scan, Arterioscler. Thromb. Vasc. Biol. 26 (2006) 597–603, https://doi.org/10.1161/01.ATV.0000201044.33220.5c.
[9] J.M. Bhasin, E. Chakrabarti, D.Q. Peng, A. Kulkami, X. Chen, J.D. Smith, Sex specific gene regulation and expression QTLs in mouse macrophages from a strain intercross, PLoS One 3 (2008), https://doi.org/10.1371/journal.pone.0001435.
[10] P. Robinet, D.M. Milewicz, L.A. Cassis, N.J. Leeper, H.S. Lu, J.D. Smith, Consideration of sex differences in design and reporting of experimental arterial pathology studies-statement from ATVB council, Arterioscler. Thromb. Vasc. Biol. 38 (2018) 292–303, https://doi.org/10.1161/ATVBAHA.117.309524.
[11] J.P. Hardwick, Cytochrome P450 omega hydroxylase (CYP4) function in fatty acid metabolism and metabolic diseases, Biochem. Pharmacol. 75 (2008) 2263–2275, https://doi.org/10.1016/j.bcp.2008.03.004.
[12] Z. Tang, S.G. Salamanca-Pinzón, Z.L. Wu, Y. Xiao, F.P. Guengerich, Human cytochrome P450 4F11: heterologous expression in bacteria, purification, and characterization of catalytic function, Arch. Biochem. Biophys. 494 (2010) 86–93, https://doi.org/10.1016/j.abb.2009.11.017.
[13] A. Kalsotra, C.M. Turman, Y. Kikuta, H.W. Strobel, Expression and characterization of human cytochrome P450 4F11: putative role in the metabolism of therapeutic drugs and eicosanoids, Toxicol. Appl. Pharmacol. 199 (2004) 295–304, https://doi.org/10.1016/j.taap.2003.12.033.
[14] V. Winslow, R. Vaivoda, A. Vasilyev, D. Dombkowski, K. Douaidy, C. Stark, J. Drake, E. Guilliams, D. Choudhary, F. Preffer, I. Stoilov, P. Christmas, Biochimica et Biophysica Acta Altered leukotriene B 4 metabolism in CYP4F18-de fi cient mice does not impact in fl ammation following renal ischemia, Biochim. Biophys. Acta Mol. Cell Biol. Lipids 1841 (2014) 868–879, https://doi.org/10.1016/j.bbalip.2014.03.002.
[15] Y. Kikuta, H. Kasyu, E. Kusunose, M. Kusunose, Expression and catalytic activity of mouse leukotriene B4ω-hydroxylase, CYP4F14, Arch. Biochem. Biophys. 383 (2000) 225–232, https://doi.org/10.1006/abbi.2000.2078.
[16] M. Fer, L. Corcos, Y. Dréano, E. Plée-Gautier, J.-P. Salaün, F. Berthou, Y. Amet, Cytochromes P450 from family 4 are the main omega hydroxylating enzymes in humans: CYP4F3B is the prominent player in PUFA metabolism, J. Lipid Res. 49 (2008) 2379–2389, https://doi.org/10.1194/jlr.M800199-JLR200.
[17] T. Yokomizo, T. Izumi, T. Shimizu, Leukotriene B4: metabolism and signal transduction, Arch. Biochem. Biophys. 385 (2001) 231–241, https://doi.org/10.1006/abbi.2000.2168.
[18] W.W. Busse, Leukotrienes and inflammation Review 2005.pdf, Am. J. Respir. Crit. Care Med. 157 (1998) 210–213, https://doi.org/10.1164/ajrccm.157.6.mar-1.
[19] Y. Kikuta, E. Kusunose, K. Endo, S. Yamamoto, K. Sogawa, Y. Fujii-Kuriyama, M. Kusunose, A novel form of cytochrome P-450 family 4 in human polymorphonuclear leukocytes: cDNA cloning and expression of leukotriene B4 omega-hydroxylase, J. Biol. Chem. 268 (1993) 9376–9380, https://doi.org/10.1299/jsmea.44.556.
[20] T.E. Dahinden, C.A. Clancy, R.M. Hugli, Stereospecificity of leukotriene B4 and structure-function relationships for chemotaxis of human neutrophils, J. Immunol. 133 (1984) 1477–1482.
[21] C.A. Clancy, M. Robert, Dahinden, T.E. Hugli, Effect of structural the chemotactic modification at carbon atom 1 of leukotriene B4 on and metabolic response of human neutrophils, Anal. Biochem. 161 (1987) 550–558.
[22] A.J. Lusis, J. Yu, S.S. Wang, The problem of passenger genes in transgenic mice, Arterioscler. Thromb. Vasc. Biol. 27 (2007) 2100–2103, https://doi.org/10.1161/ATVBAHA.107.147918.